Joint Special Interest Group meeting between euspen and ASPE
Dimensional Accuracy and Surface Finish in Additive Manufacturing,
KU Leuven, BE, October 2017
www.euspen.eu

Uncertainty Quantification of an X-ray Computed Tomography System

J. Cuadra[1], C. Divin[1], R. Panas[1]

[1]*Lawrence Livermore National Laboratory, Livermore, CA, United States of America*

Abstract

Newly manufactured complex 3D parts, such as additively manufactured, with internal features often failed to meet the standards due the presence of uncontrolled process variations. An optimal solution that can perform standardized methods of quality control and accurate metrology of these parts is X-ray Computed Tomography (XCT). However, XCT measurements are influenced by various parameters resulting in additional error sources, which are not present in conventional techniques including optical and tactile methods. Such uncertainties are common when acquiring the XCT data and post processing it by using tomographic reconstruction algorithms. For instance, the error sources associated with the environment, X-ray source, detector and other components include the temperature, humidity, mechanical vibrations, and others. In this paper, a new model to quantify the uncertainty from the dominant error sources at each data acquisition hardware component is presented. The ongoing modeling effort focuses on uncertainties in the object transmission value measured at a single pixel, which is a 0D point at the detector. This 0D uncertainty model is applied to a commercial X-ray systems for uncertainty quantification by acquiring the intensity (flux) of the X-ray source, dark field counting noise, mechanical and temperature fluctuations, thermal sensitivities coefficients, scattering, cross-talk factor, and after glow response. The results of this study could potentially provide critical information for establishing and optimizing XCT system for metrology applications.

Introduction

X-ray Computed Tomography (XCT) is an optimal nondestructive method for various applications including three major fields: medical imaging, characterization of materials, and dimensional and quality control assessments of manufactured parts [1]–[3]. Its increasing demand in manufacturing applications is due to the capability to nondestructively provide the measurement of inaccessible internal features of manufactured as well multi-material components and assembled parts permitting both dimensional and material quality assessment in a single task [4], [5] . Although its applicability in the medical and characterization fields meets the basic requirements, this is not the case for dimensional CT metrology since the accuracy and spatial resolution requirements and standards tend to be higher [1], [2], [6]. Furthermore, the X-ray CT measurements are influenced by many different parameters resulting in additional error sources to those in traditional techniques such as coordinate measuring machines (CMMs) or optical methods. Such errors and uncertainties are intrinsic of the experimental setup and the tomographic reconstruction algorithms implemented for data post-processing. Some of these error sources in the environment, x-ray source, detector and other components include the temperature, humidity, mechanical vibrations, beam hardening effects, quantum efficiency, threshold determination, and others [1], [6]–[8]. A new uncertainty model that attempts to characterize and quantify the dominant sources of error in each data acquisition hardware component is presented herein with the main objective of optimizing the X-ray CT systems for metrology applications.

Methodology

The model developed herein takes into account the contributions to signal variation as measured at a single pixel, including uncertainties and sensitivities from different data acquisition XCT system components and it implements a systems approach [9]. The 0D model is applied to a specific XCT system and it considers only errors which have no larger scale form, and thus does not require higher dimensional modelling. Inasmuch, the object is assumed to be a block of uniform thickness from the perspective of the studied pixel 'point' on the

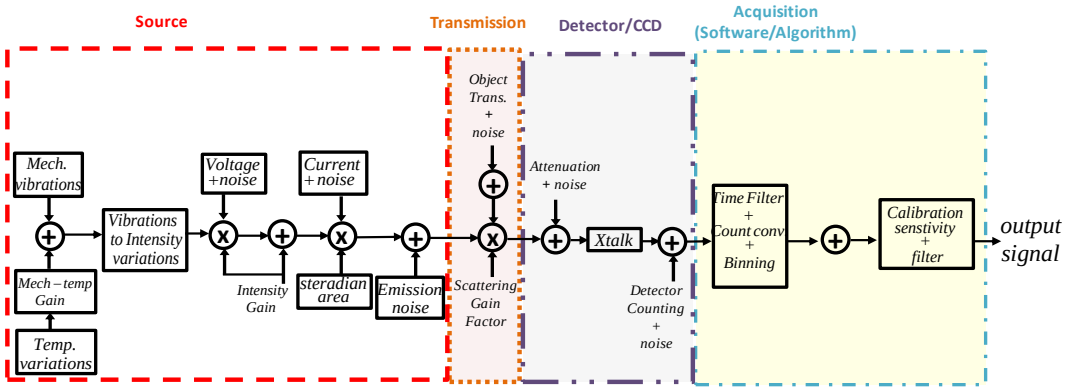

Figure 1: Graphical representation of sources of error for a conventional XCT system.

detector and quantify its corresponding uncertainty. Figure 1 displays the overall parameters included in the model for each XCT system component in the form of a signal variation flow graph. For instance, the source includes mechanical vibrations at the source and with respect to the detector, ambient and component temperature effects, electrical current noise and source emission variation which could affect the final emission of X-rays before they are recorded by the detector. Similarly, other sources of noises are acquired in the transmission and detector components since the object attenuation and scattering as well as the efficiency and count noise of the detector affect the final output signal. The signal variation flow graph also captures effects due to detector pixel cross talk, afterglow response, dark field offset (i.e. background noise of the detector) and a binning parameter in addition to a calibration term that normalizes the final response of the model output signal (Ψm).

$$\begin{aligned}\psi_m = ((((&\sigma_{emission} + (G_{intensity} + (\sigma_{mech} + \sigma_{temp}\alpha_{mech/temp})\cdot \\ &\alpha_{\Delta intensity/mech} + \sigma_{voltage}\cdot\alpha_{\Delta intensity/voltage})(\sigma_{current} + I))\cdot \\ &\eta_o + \sigma_{\eta o})G_{scattering}\eta_{eff} + \sigma_{\eta eff})G_{cross talk} + \sigma_{detector noise})\cdot \\ &G_{binning}t_{exposure}\end{aligned} \quad (1)$$

where σ, G, α, I, η_o, η_{eff} and t represent sources of error, gain factor, conversion coefficients, current, attenuation value, detector intrinsic efficiency and time. Furthermore, the signal variation flow graph depicts the use of low and high pass filtering to create a bandwidth of the uncertainty in terms of variance as a function of frequency. The variance is obtained by calculating the power spectral density function since the time measurements are treated as random processes and its statistical characteristics can only be described by the power of the noise instead of the amplitude (i.e. conventional Fourier Transform). The detailed variables used in XCT system source component of the model are depicted in Equation (2). This component of the model can be simplified to:

$$r_{ps} = \sigma_{ns} + (1+\sigma_\Omega)\Omega G_S\begin{pmatrix}1+\alpha_{Gs\theta x}\sigma_{G\theta x} + \alpha_{Gs\theta y}\sigma_{G\theta y} + \\ \alpha_{GsVs}\sigma_V\end{pmatrix}\cdot (\sigma_I + I_s) \quad (2)$$

where Ω is the pixel solid angle as a function of the source coordinates, G_S is the X-ray intensity (flux) gain factor term, I_S is the current (for the case of electrically driven sources), σ_{ns}, σ_I, $\sigma_{G\theta x}$, $\sigma_{G\theta y}$, σ_Ω and σ_V are the noise parameters for the emission variation, current, angular variation in θx and θy, pixel solid angle variation and voltage, respectively. Equation (2) also includes $\alpha_{Gs\theta x}$, $\alpha_{Gs\theta y}$, and α_{GsV} which are the sensitivity coefficients for the angular variations in θx and θy in addition to the source voltage. This model for the XCT source also includes temperature variations and sensitivity coefficients which are comprised in the angular and pixel solid angle variations. The final output for Source model is r_{ps} which is the count rate produced by the XCT source. In the case of the model for the material/object transmission effects, the number of uncertainties includes a binomial noise from attenuation term ($\sigma_{\eta o}$), a specific transmission parameter value (η_o) of the object and a gain factor associated to scattering (G_{so}). The output signal, r_{po}, in count rate units for the transmission section can be represented by:

$$r_{po} = (\sigma_{\eta o} + \eta_o r_{ps})G_{so} \quad (3)$$

The output of the source or material/object transmission model, i.e. r_{ps} and r_{po} correspondingly, may be the input for an optical filter model with an output signal r_{pf}. This optical filter model is basically the material/object transmission model without any scattering term and it describes the count rate attenuation due to an optical filter. Moreover, any other type of filtering can be treated similarly by applying an additional transmission model. The model applied for the detector component describes the uncertainty measured by the noise due to the intrinsic efficiency ($\sigma_{\eta I}$) and counts (σ_{ndc}) of the system. In the model, the zero mean variations (unbiased) relative to a parameter are represented as σ while biases relative to the parameter value upon system calibration are denoted as Δ. The systemic error due to the offset from the counts (Δ_{ndc}), a cross talk factor (G_{ct}), a detector dynamics filter (F_d) and the count rate signal from either the object transmission (r_{po}) are included in the XCT detector model. The final signal yields (r_{pd}) in counts per second:

$$r_{pd} = \sigma_{ndc} + \Delta_{ndc} + G_{ct}F_d(\sigma_{\eta I} + \eta_I \cdot r_{po}) \quad (4)$$

Ultimately, the final output signal of the X-ray system is obtained by passing the signal from r_{pd} through a binning factor

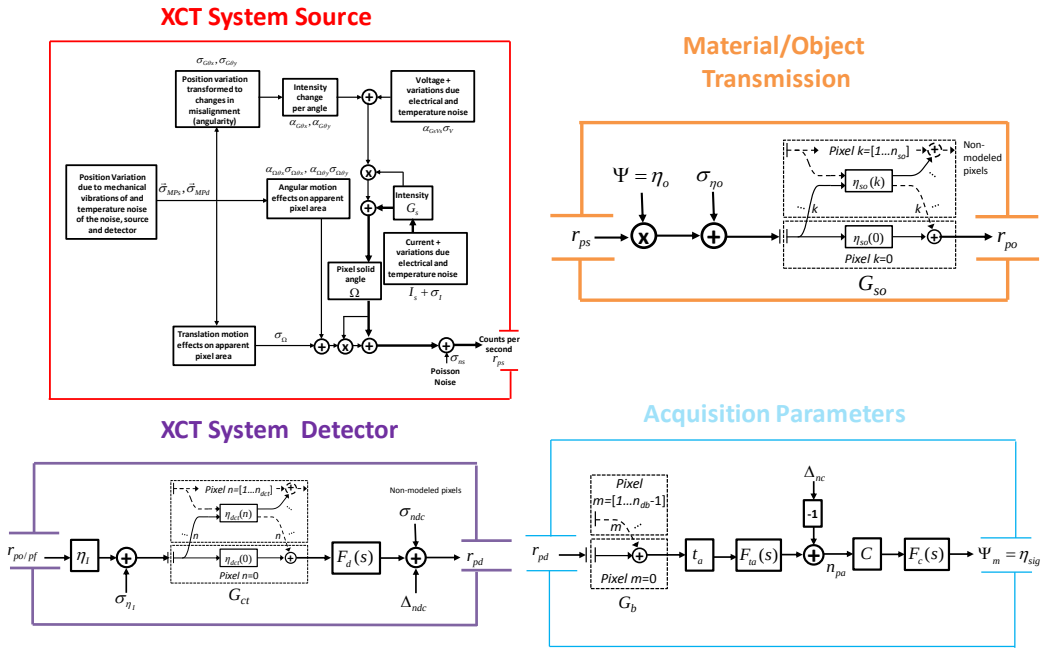

Figure 2: Signal variation flow graphs for all X-ray data acquisition components.

(G_b), converting it to counts by multiplying by the acquisition time (also referred as exposure time, t_a) as well as factoring a low pass filter (F_{ta}), applying a calibration offset (Δ_{nc}) and calibration factor (C) as well as implementing a high pass filter (F_C) adjusted by the time interval between system calibrations. The final equation (n_{sig}) gives an attenuation signal:

$$n_{sig} = F_C(s)C(-\Delta_{nc} + F_{ta}(s)t_a G_b r_{pd}) \quad (5)$$

The power spectral density function of each noise, $S_n(f)$, is scaled by their respective frequency dependent sensitivities and geometrically summed to obtain the full system noise spectral density:

$$S_{\psi m}(f) = \sum_n \left| \frac{\partial \psi_m(2\pi i f)}{\partial \sigma_n} \right|^2 S_n(f) \quad (6)$$

An estimate of the noise variance is calculated by integrating the system spectral noise density over a frequency range. Then, the total uncertainty is expressed as

$$\sigma_{\psi m} = \sqrt{\int_{f_{\min}}^{f_{\max}} S_{\psi m}(f)\partial f} \quad (7)$$

The inputs for the model provided by the user include both specific parameters from the XCT setup and spatial and time varying intensity and noise parameters as well as sensitivity coefficients. For instance, the setup parameters include exposure time, source-to-detector distance, current, and others. On the other hand, the intensity is measured on plane perpendicular to the X-ray path; and noise parameters are sources of error which are characteristic of the acquisition and thus need to be measured. These parameters consist of the mechanical vibrations, temperature variations and sensitivity coefficients, and others. Hence, the model requires in total 7 experimental measurements to apply the uncertainty model for a given XCT system. These measurements are essentially inputs for the time variations and sensitivities related to motion, temperature, intensity, and other types of noises. These experimental procedures include: (i) characterizing the X-ray source intensity, (ii) dark field counting noise, (iii) temperature fluctuations and thermal sensitivities, (iv) electrical potential and current fluctuations, (v) scattering measurements, (vi) pixel dynamics parameters and (vii) mechanical vibrations.

Preliminary results and discussion

The preliminary results consist of data acquired from 3 out of the 7 experimental measurements and uncertainty maps at each XCT component. The measurements for the model were obtained from a commercial system from *Zeiss Xradia*.

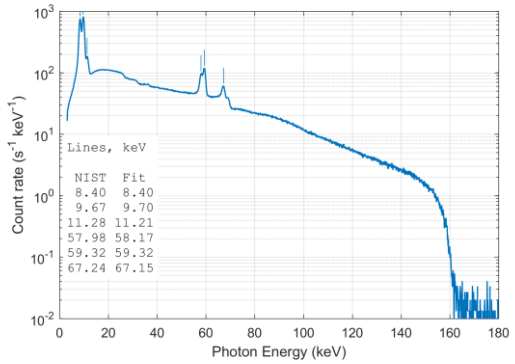

Figure 3: X-ray system spectrum for 160 kV at 0.3 W.

The first set of results were obtained from the X-ray flux intensity. These results involved using a X-123CdTe Amptek X-ray spectrometer (i.e. a single pixel detector) to measure both the spectral response and intensity for a 60 second exposure time and a 160 kV at 0.3 W energy and power level. The flux was limited by the aperture of the single pixel detector. The 2048 channels in the detector were calibrated using the characteristic lines (shown in a table on the plot) of a tungsten anode. The bremsstrahlung X-ray source spectrum is shown in Figure 3 in units of count rate per keV. The intensity is the spatial average of the flux measured at positions on the plane perpendicular to the X-ray path. Figure 3 also depicts a decay as the energies get higher. Similarly, this trend is shown for the intensity spatial distribution shown in Figure 4. A 15 x 7 mosaic-type measurement was implemented to measure the flux at each of these plane coordinates. The characteristic spot is depicted evidently for 15 keV and 60 keV, while at higher energies this spot seems to be diverging due to low count rate values.

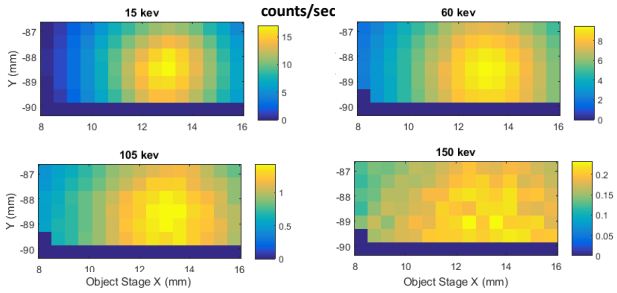

Figure 4: XCT system source map for a given energy level.

Another key measurement for the model is recording the thermal noise and sensitivity. All thermal effects relate to any motions or thermal expansion that could occur in the XCT components due temperature variations. Figure 5 displays the temperature spectral density functions at different hardware components of the XCT system. These measurements were taken in 10 second intervals for a duration of 48 hour using thermocouples. The results show that the thermal response is comparable to low pass filter. Another experiment regarding the temperature measurements is the thermal sensitivity of the XCT system which is performed by varying temperature and recording the displacements.

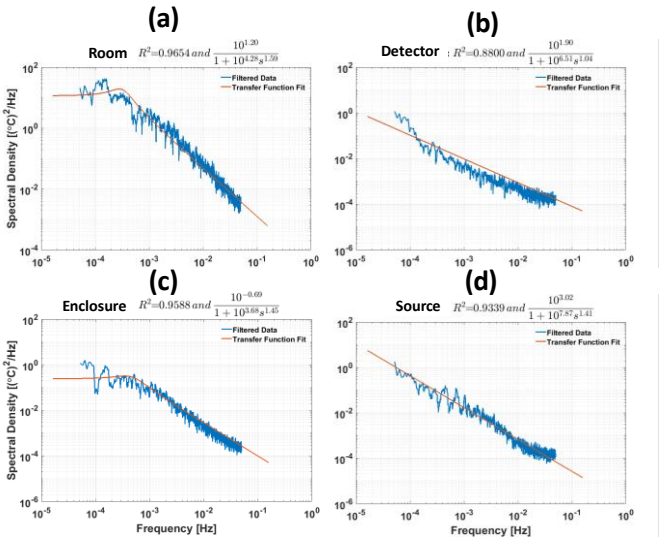

Figure 5: XCT system thermal spectral density response from (a) the room, (b) detector, (c) enclosure, and (d) source.

The temperature variations are converted into motion which is then added to the mechanical vibrations of the components. This vibration analysis is recorded using triaxial accelerometers. Figure 6 shows the spectral density functions for 3 translational components of the vibrations. The X- and Y- axes have a comparable behavior which shows flicker noise at low

frequencies. On the hand, the Z-axis behaves as a low pass filter similar to the thermal response in Figure 5.

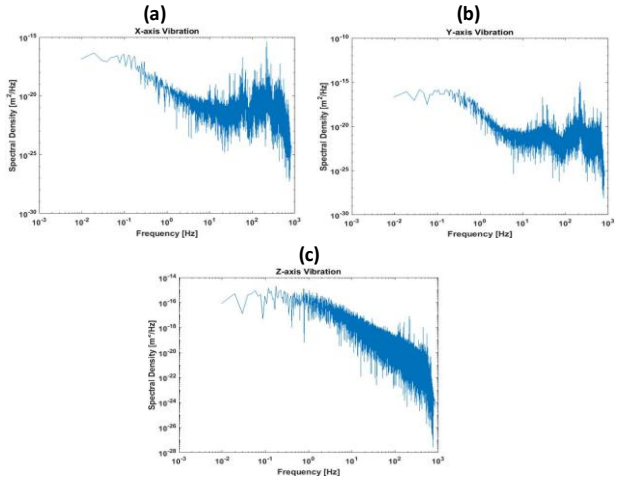

Figure 6: XCT system vibration spectral density response from (a) X-, (b) Y- and (c) Z-axes.

In the model, all motions are measured from vibrations and temperature variations and then based on a source-detector distance are used to calculate misalignment on the intensity G_S and any effects on the pixel solid angle Ω. These preliminary results associated with intensity and noise are the inputs for the model. In addition, these results offer an insight into the magnitude and response of the intensity as well as some of the noise inputs. To capture and provide an outlook into how the model performs, a trial run on a customized micro CT system from LLNL [10] was performed.

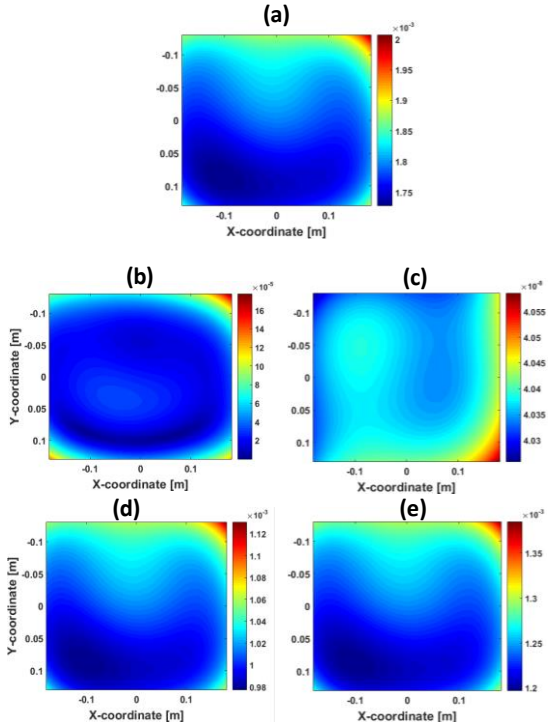

Figure 7:Uncertainty field for (a) the total noise of the XCT system, (b) mechanical vibrations, (c) temperature variations, (d) emission noise and (e) object transmission

Some of the input noises were extracted from [9] and these included spectral density functions for the mechanical vibrations, temperature effects and voltage noise. On the other hand, the current, exposure time, pixel area, source to detector distance as well as the measured bright and dark background field were obtained from an experimental setup for the micro CT. Figure 5a shows the total uncertainty from the system calculated by adding all the uncertainty components which denotes the confidence bounds to the unitless attenuation signal. The total uncertainty can be divided into different components. For instance, the uncertainty of all mechanical vibrations is depicted in Figure 5b. Similarly, the temperature variations, emission and transmission, which the latter two are the most dominant components of the uncertainty.

Conclusion

The preliminary results provided an insight into the intensity and some of the noise responses of a commercial XCT system. The results also included the total uncertainty on pixel coordinates, for a specific micro CT system at a given energy level and characteristic acquisition parameters. Both results are essential for precision metrology applications since they are informative data that can potentially identify dominant sources of error with the goal of improving the performance of the XCT system measurements. Furthermore, the uncertainty model will be extended from 0D (single pixel) to higher dimensional uncertainties with a target of mapping the full range of variation observed in XCT measurements.

Acknowledgements

This work was performed under the auspices of the U.S. Department of Energy by Lawrence Livermore National Laboratory under Contract DE-AC52-07NA27344. LLNL-CONF-733872.

References

[1] S. Carmignato, D. Dreossi, L. Mancini, F. Marinello, G. Tromba, and E. Savio, “Testing of x-ray microtomography systems using a traceable geometrical standard,” *Meas. Sci. Technol.*, vol. 20, no. 8, p. 084021, 2009.

[2] J. P. Kruth, M. Bartscher, S. Carmignato, R. Schmitt, L. De Chiffre, and A. Weckenmann, “Computed tomography for dimensional metrology,” *CIRP Ann. - Manuf. Technol.*, vol. 60, no. 2, pp. 821–842, 2011.

[3] P. Shah, R. Racasan, and P. Bills, “Comparison of Different Additive Manufacturing Methods Using Optimized Computed Tomography,” *6th Conf. Ind. Comput. Tomogr.*, 2016.

[4] H. Villarraga, C. Lee, T. Corbett, J. A. Tarbutton, and S. T. Smith, “Assessing additive manufacturing processes with X-ray CT metrology,” in *American Society for Precision Engineering, ASPE*, 2015.

[5] H. Villarraga, C. Lee, S. P. Charney, J. A. Tarbutton, and S. T. Smith, “Dimensional metrology of complex inner geometries built by additive manufacturing,” in *American Society for Precision Engineering, ASPE*, 2015.

[6] S. Carmignato, A. Pierobon, P. Rampazzo, M. Parisatto, and E. Savio, “CT for Industrial Metrology – Accuracy and Structural Resolution of CT Dimensional Measurements,” *Conf. Ind. Comput. Tomogr.*, pp. 161–172, 2012.

[7] S. Carmignato, “Computed tomography as a promising solution for industrial quality control and inspection of castings,” *Metall. Sci. Technol.*, vol. 30, no. 1, pp. 5–14, 2012.

[8] S. Carmignato, “Accuracy of industrial computed tomography measurements: Experimental results from an international comparison,” *CIRP Ann. - Manuf. Technol.*, vol. 61, no. 1, pp. 491–494, 2012.

[9] R. M. Panas, M. A. Cullinan, and M. L. Culpepper, “Design of piezoresistive-based MEMS sensor systems for precision microsystems,” *Precis. Eng.*, vol. 36, no. 1, pp. 44–54, 2012.

[10] I. M. Seetho, W. D. Brown, J. S. Kallman, H. E. Martz, and W. T. White, “MicroCT: Automated Analysis of CT Reconstructed Data of Home Made Explosive Materials Using the Matlab MicroCT Analysis GUI,” LLNL-TR-503291,(October 6, 2011), 2011.